A human importin-β-related disorder: Syndromic thoracic aortic aneurysm caused by bi-allelic loss-of-function variants in *IPO8*

Ilse Van Gucht,[1,29] Josephina A.N. Meester,[1,29] Jotte Rodrigues Bento,[1] Maaike Bastiaansen,[1] Jarl Bastianen,[1] Ilse Luyckx,[1,2] Lotte Van Den Heuvel,[1] Cédric H.G. Neutel,[3] Pieter-Jan Guns,[3] Mandy Vermont,[3] Erik Fransen,[1,4] Melanie H.A.M. Perik,[1] Joe Davis Velchev,[1] Maaike Alaerts,[1] Dorien Schepers,[1,5] Silke Peeters,[1] Isabel Pintelon,[6] Abdulrahman Almesned,[7] Matteo P. Ferla,[8] Jenny C. Taylor,[8] Anthony R. Dallosso,[9] Maggie Williams,[9] Julie Evans,[9] Genomics England Research Consortium, Jill A. Rosenfeld,[10,11] Thierry Sluysmans,[12] Desiderio Rodrigues,[13] Ashish Chikermane,[14] Gangadhara Bharmappanavara,[15] Kayal Vijayakumar,[16] Hassan Mottaghi Moghaddam Shahri,[17] Narges Hashemi,[18] Paria Najarzadeh Torbati,[19] Mehran B. Toosi,[20] Zuhair N. Al-Hassnan,[21] Julie Vogt,[22] Nicole Revencu,[23] Isabelle Maystadt,[24] Erin M. Miller,[25] K. Nicole Weaver,[26] Amber Begtrup,[27] Henry Houlden,[28] David Murphy,[28] Reza Maroofian,[28] Alistair T. Pagnamenta,[8] Lut Van Laer,[1] Bart L. Loeys,[1,2,29,*] and Aline Verstraeten[1,29,*]

Summary

Importin 8, encoded by *IPO8*, is a ubiquitously expressed member of the importin-β protein family that translocates cargo molecules such as proteins, RNAs, and ribonucleoprotein complexes into the nucleus in a RanGTP-dependent manner. Current knowledge of the cargoes of importin 8 is limited, but TGF-β signaling components such as SMAD1–4 have been suggested to be among them. Here, we report that bi-allelic loss-of-function variants in *IPO8* cause a syndromic form of thoracic aortic aneurysm (TAA) with clinical overlap with Loeys-Dietz and Shprintzen-Goldberg syndromes. Seven individuals from six unrelated families showed a consistent phenotype with early-onset TAA, motor developmental delay, connective tissue findings, and craniofacial dysmorphic features. A C57BL/6N *Ipo8* knockout mouse model recapitulates TAA development from 8–12 weeks onward in both sexes but most prominently shows ascending aorta dilatation with a propensity for dissection in males. Compliance assays suggest augmented passive stiffness of the ascending aorta in male $Ipo8^{-/-}$ mice throughout life. Immunohistological investigation of mutant aortic walls reveals elastic fiber disorganization and fragmentation along with a signature of increased TGF-β signaling, as evidenced by nuclear pSmad2 accumulation. RT-qPCR assays of the aortic wall in male $Ipo8^{-/-}$ mice demonstrate decreased *Smad6/7* and increased *Mmp2* and *Ccn2* (*Ctgf*) expression, reinforcing a role for dysregulation of the TGF-β signaling pathway in TAA development. Because importin 8 is the most downstream TGF-β-related effector implicated in TAA pathogenesis so far, it offers opportunities for future mechanistic studies and represents a candidate drug target for TAA.

Thoracic aortic aneurysm (TAA) refers to a pathological and progressive dilatation of the aorta that, if left untreated, imposes a risk for life-threatening aortic dissection or rupture. TAA presents either as an isolated condition (non-syndromic TAA) or as part of a multi-systemic connective tissue disorder (syndromic TAA). Most typically,

[1]Center of Medical Genetics, University of Antwerp and Antwerp University Hospital, Edegem 2650, Belgium; [2]Department of Human Genetics, Radboud University Nijmegen Medical Center, Nijmegen 6525 GA, the Netherlands; [3]Laboratory of Physiopharmacology, University of Antwerp, Antwerp 2610, Belgium; [4]StatUa Center for Statistics, University of Antwerp, Antwerp 2000, Belgium; [5]Laboratory of Molecular, Cellular and Network Excitability, Department of Biomedical Sciences, University of Antwerp, Antwerp 2610, Belgium; [6]Laboratory of Cell Biology & Histology, Department of Veterinary Sciences, University of Antwerp, Antwerp 2610, Belgium; [7]Prince Sultan Cardiac Centre, Qassim 31982, Saudi Arabia; [8]NIHR Oxford Biomedical Research Centre, Wellcome Centre for Human Genetics, University of Oxford, Oxford OX3 7BN, UK; [9]Bristol Genetics Laboratory, South West Genomic Laboratory Hub, Southmead Hospital, Bristol BS10 5NB, UK; [10]Department of Molecular and Human Genetics, Baylor College of Medicine, Houston, TX 77030, USA; [11]Baylor Genetics Laboratories, Houston, TX 77021, USA; [12]Department of Pediatric Cardiology, Cliniques Universitaires Saint-Luc, University of Louvain, Brussels 1200, Belgium; [13]Birmingham Women's and Children's Hospital NHS Foundation Trust, Steelhouse Lane, Birmingham B4 6NH, UK; [14]Birmingham Women & Children's Hospital, Birmingham B4 6NH, UK; [15]Musgrove Park Hospital, Somerset NHS Foundation Trust, Taunton TA1 5DA, UK; [16]Department of Paediatric Neurology, University Hospitals Bristol NHS Foundation Trust, Bristol BS2 8BJ, UK; [17]Pediatric Department, Faculty of Medicine, Mashhad University of Medical Sciences, Mashhad 009851, Iran; [18]Department of Pediatric Neurology, School of Medicine, Mashhad University of Medical Sciences, Mashhad 009851, Iran; [19]Department of Molecular Genetics, Next Generation Genetic Polyclinic, Mashhad University of Medical Sciences, Mashhad 009851, Iran; [20]Department of Pediatric Neurology, Ghaem Hospital, Mashhad University of Medical Sciences, Mashhad 009851, Iran; [21]Cardiovascular Genetic Program, Department of Medical Genetics, King Faisal Specialist Hospital and Research Centre, Riyadh 11564, Saudi Arabia; [22]West Midlands Regional Genetics Service, Birmingham Women's and Children's Hospital, Birmingham, B15 2TG, UK; [23]Center for Human Genetics, Cliniques Universitaires Saint-Luc, University of Louvain, Brussels 1200, Belgium; [24]Centre de Génétique Humaine, Institut de Pathologie et de Génétique, Gosselies (Charleroi) 6041, Belgium; [25]The Heart Institute, Department of Pediatrics, Cincinnati Children's Hospital Medical Center and University of Cincinnati College of Medicine, Cincinnati, OH 45229, USA; [26]Division of Human Genetics, Department of Pediatrics, Cincinnati Children's Hospital Medical Center and University of Cincinnati College of Medicine, Cincinnati, OH 45229, USA; [27]GeneDx, Gaithersburg, MD 20877, USA; [28]Department of Neuromuscular Disorders, UCL Queen Square Institute of Neurology, London, WC1N 3BG, UK
[29]These authors contributed equally
*Correspondence: aline.verstraeten@uantwerpen.be (A.V.), bart.loeys@uantwerpen.be (B.L.L.)
https://doi.org/10.1016/j.ajhg.2021.04.019.

the inheritance pattern is autosomal dominant, but rare X-linked or autosomal recessive families have also been reported. Because pathogenic variants in the more than 30 known TAA-associated genes explain less than 30% of probands with a positive family history,[1] additional TAA-associated genes remain to be identified.

Important mechanistic insights into syndromic TAA formation have largely emanated from elucidation of the etiology of two clinically overlapping autosomal dominant TAA syndromes: Marfan syndrome (MFS [MIM: 154700]) and Loeys-Dietz syndrome (LDS [MIM: 609192, 610168, 613795, 614816, and 615582]).[2] Besides TAA, MFS is characterized by ocular (e.g., ectopia lentis), skeletal (e.g., overgrowth, pectus deformity), and cutaneous (e.g., striae, hernia) manifestations. LDS can be distinguished from MFS by the unique presence of hypertelorism, cleft palate or bifid uvula, and prominent arterial tortuosity, as well as by a more widespread and severe aneurysm phenotype. Whereas MFS is caused by dominant-negative or haploinsufficient variants in the extracellular matrix (ECM) component fibrillin 1[3] (*FBN1* [MIM: 134797]), LDS results from loss-of-function variants in six key components of the canonical transforming growth factor β (TGF-β) signaling pathway (i.e., TGFBR1/2 [MIM: 190181 and 190182], SMAD2/3 [MIM: 601366 and 603109], TGFB2/3 [MIM: 190220 and 190230]) (Figure S1).[4–10] In both conditions, analysis of the aortic wall in mouse models and affected individuals shows a clear tissue signature for enhanced TGF-β signaling, including activation of signaling intermediates and increased output of TGF-β target genes.[11] Interestingly, a third condition with extensive phenotypic overlap with MFS and LDS but less severe cardiovascular involvement and the unique presence of neurodevelopmental delay (Shprintzen-Goldberg syndrome [SGS] [MIM: 182212]) is caused by heterozygous missense variants located in the R-SMAD-binding domain of a negative regulator of the TGF-β transcriptional response called SKI (*SKI* [MIM: 164780]) (Figure S1).[12,13]

Using exome or genome sequencing in six unrelated probands presenting with an LDS/SGS-like phenotype (for details, see supplemental materials and methods), we identified bi-allelic loss-of-function variants in *IPO8* (MIM: 605600; GenBank: NM_006390.3), encoding the nuclear import protein importin 8 (Figures 1A and S2). None of the probands carried a likely pathogenic variant in any of the known TAA-associated genes. Except for p.Leu866Profs*12 (c.2597_2601delTTTTC) (1/250,920 alleles), all identified variants are absent from the Genome Aggregation Database (gnomAD v.2.1.1). Causality is further supported by segregation analysis, which demonstrated heterozygosity in the unaffected parents and siblings (Figure 1A) as well as homozygosity in one additional affected brother (individual 4-II:3; Figure 1A). Subsequent Sanger sequencing of the coding regions of *IPO*8 in 50 other genetically unsolved MFS-, LDS-, or SGS-like probands did not reveal additional individuals with homozygous or compound heterozygous variants.

Recurrent phenotypic manifestations in our series of individuals with bi-allelic *IPO8* variants include facial dysmorphism with dolichocephaly (5/7), frontal bossing (6/7), hypertelorism (6/7), eyelid ptosis (4/7), retrognathia (6/7), and a high arched (6/7) or cleft palate/bifid uvula (3/7); skeletal findings with arachnodactyly (6/7), joint hypermobility (7/7), pectus excavatum (7/7), foot deformity (5/7), and scoliosis (3/7); neuromuscular features, including hypotonia (7/7) and developmental delay (7/7); cardiovascular abnormalities with aortic root and/or ascending aortic aneurysm (6/7) and structural heart disease (atrial or ventricular septal defect [ASD or VSD, respectively] and patent ductus arteriosus [PDA]) (7/7); and finally, umbilical and/or inguinal hernia (5/7) (Figure 1B, Table 1). No disproportionate body growth was observed (Figure S3). Of note, despite the severe aneurysm phenotype, none of the affected individuals experienced an arterial or aortic dissection, but this may be due to their young age. Additionally, marked arterial tortuosity, a typical LDS feature, was reported in two affected individuals (2-II:1 and 6-II:1) but might have been overlooked in the others because they have not yet undergone head-to-pelvis arterial imaging. Overall, the phenotype fits in the spectrum of LDS/SGS-like disorders (Table 2).

Six out of eight *IPO8* variants are predicted to result in a premature termination codon and, as a result, to induce nonsense-mediated mRNA decay (NMD). Indeed, in fibroblast cDNA of individual 3-II:3, c.2597_2601delTTTTC was only observed upon puromycin treatment (Figure S4A). In blood-derived cDNA of the same child, c.1428+5G>A was found to result in exon 13 skipping (Figures S5A and S5B). *In silico* protein modeling of its predicted resultant in-frame deletion, p.Lys447_Arg476del (c.1428+5G>A), suggests abnormal folding due to removal of a single helix (Figure S5C). In fibroblast cDNA of individual 1-II:3, the variant allele was seen even in the absence of inhibition of NMD with puromycin, revealing surprising escape from NMD (Figure S4B). No protein was seen in immunoblotting on fibroblast lysates of individuals 1-II:3 and 3-II:3 via an antibody against the N-terminal portion of importin 8, in keeping with a loss-of-function mechanism (Figure S4C). In proband 1-II:3, the lack of importin 8 protein is possibly attributed to translational repression, which previously has been described in other conditions,[15] or significant protein instability. For individual 6-II:1, fibroblasts are not available, but *in silico* modeling of the predicted resultant deletion-insertion, p.Thr967_Glu1006delinsLys (c.2900−1G>A), suggests removal of the last structured part of the protein (Figure S6), which based on this region's role in controlling the protein conformation in some other β-importins, may significantly affect protein stability.[16–18]

Murine importin 8 is 92% identical and 95% similar to its human ortholog, rendering mice a suitable animal model to pursue supportive *in vivo* evidence for a causal relationship between *IPO8* deficiency and TAA. We used a C57BL/6N *Ipo8*$^{-/-}$ model that was previously only known to

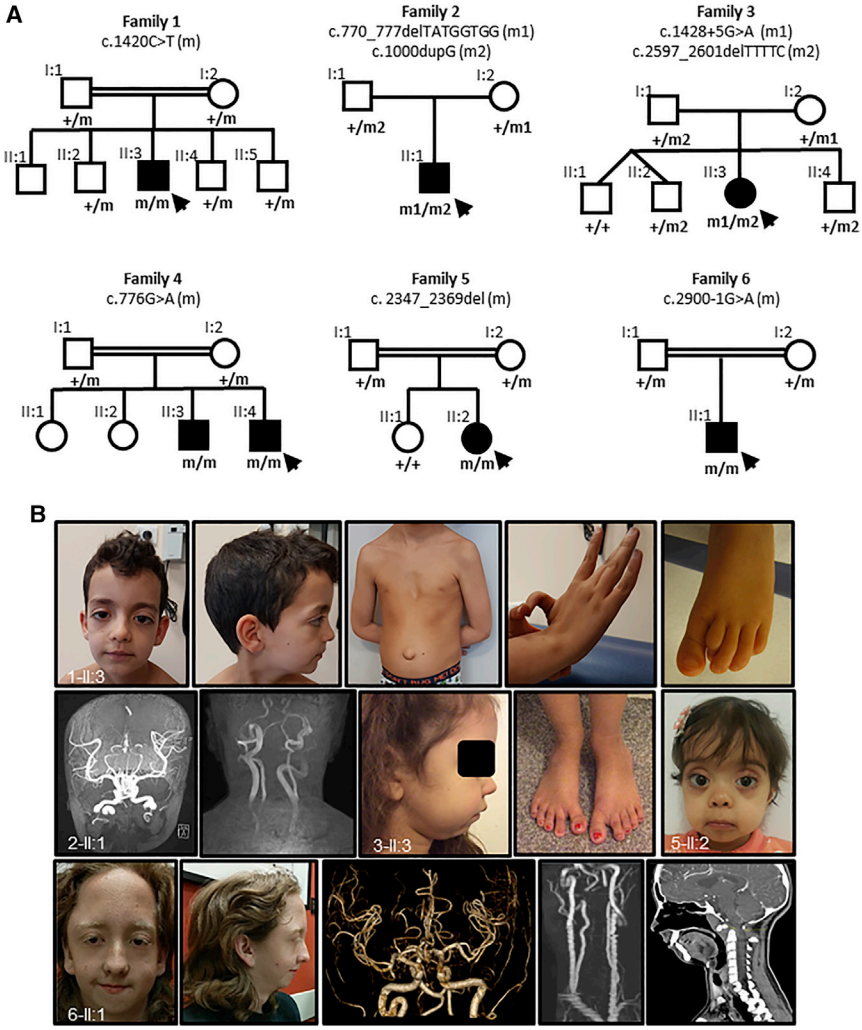

Figure 1. Familial screening and clinical characterization of individuals with bi-allelic *IPO8* variants

(A) Pedigrees of the families with their respective pathogenic variants. Squares represent males, while circles represent females, filled symbols denote affected individuals, a double line connecting spouses symbolizes consanguinity, and m/m1/m2 denote the presence of the respective *IPO8* variants and a + sign represents the wild-type *IPO8* allele. Variants are annotated against GenBank: NM_006390.3.

(B) Clinical phenotyping. Proband 1-II:3 showing prominent forehead, hypertelorism, mild ptosis left eye, retrognathia, pectus excavatum, umbilical hernia, joint hypermobility with thumb abduction, and camptodactyly of the second toe. CT angiography of proband 2-II:1 demonstrating dilatation of the common carotid arteries along with marked tortuosity of the common carotid and internal carotid artery, mild tortuosity of the vertebral arteries, and enlargement of the anterior and middle cerebral arteries bilaterally. Proband 3-II:3 presenting with frontal bossing with bitemporal flattening, retrognathia, downturned corners of the mouth, and flat feet. Proband 5-II:2 showing prominent forehead, significant hypertelorism with flat nasal bridge, mild ptosis of left eye, and retrognathia. Proband 6-II:1 demonstrating dolichocephaly, retrognathia, malar flattening, downslanting palpebral fissures, and hypertelorism. Magnetic resonance angiography (MRA) revealing tortuous intracranial and extracranial arterial vessels, most prominently involving the superior cervical internal carotid arteries with dilation of the left internal carotid artery at the carotid bifurcation. CT scan (pre-surgical) showing os odontoideum with cervical spinal canal stenosis (arrows).

present with reduced grip strength and diminished vertical activity, suggesting muscle weakness and decreased locomotor exploration, respectively,[19] and thus corroborating with the observed hypotonia and (possibly associated) motor delay in individuals with *IPO8* bi-allelic variants. Serial transthoracic echocardiography (age 4–32 weeks) of the aortic root at the level of the sinuses of Valsalva and distal ascending aorta in *Ipo8*$^{-/-}$ mice and their wild-type (WT) littermates (N = 17/group) revealed statistically significant progressive dilatation in mutant mice at both anatomical locations, and aneurysms of the distal ascending aorta were already becoming visible at the age of 8–12 weeks (p_{root} = 1.3E−3 [Figure 2A]; p_{asc} = 8.4E−9 [Figure 2B]). Intriguingly, sex-stratified analyses demonstrated aortic root enlargement in both mutant females (7 *Ipo8*$^{-/-}$ versus 8 WT; p_{root_f} = 2.3E−3 [Figure S7A]) and males (10 *Ipo8*$^{-/-}$ versus 9 WT; p_{root_m} = 2.3E−2 [Figure S7B]), whereas the ascending aortic aneurysm phenotype is very pronounced and only statistically significant in the male *Ipo8*$^{-/-}$ animals (p_{asc_f} = 6.5E−2 [Figure S7C] versus p_{asc_m} = 8.4E−10 [Figure 2C]). After the last echo at 32 weeks, 14 *Ipo8*$^{-/-}$ and 17 WT animals were kept alive until the age of 48 weeks. Of these, three homozygous mutant males (3/9, 33.3%) died from an aortic rupture at the age of 32, 36, and 46 weeks, while no aortic rupture-related mortality was seen in the homozygous females (0/5, 0%) or WT animals (0/17, 0%). Sex differences in syndromic TAA penetrance and severity have been reported before, both in mice and humans.[20,21] Generally, males are more severely affected, exhibiting larger aortas and experiencing dissection and/or rupture more frequently.[22,23] Several studies in TAA mouse models have attempted to define the basis for the observed sex differences, revealing a context-dependent role for female and male hormone signaling, hypertension, and/or exacerbated ERK activation, but no predominant mechanism has been identified.[21] The C57BL/6N *Ipo8*$^{-/-}$ mouse model represents a promising tool to further investigate the TAA sexual dimorphism. Of note, during our echocardiography studies, we did not observe severe structural outflow tract

Table 1. Detailed overview of the clinical characteristics of individuals with bi-allelic *IP08* variants

	Family 1, proband 1-II:3	Family 2, proband 2-II:1	Family 3, proband 3-II:3	Family 4, proband 4-II:4	Family 4, individual 4-II:3	Family 5, proband 5-II:2	Family 6, proband 6-II:1
Variant c. annotation	c.1420C>T, homz	c.[770_777delT ATGGTGG]; [1000dupG]	c.[1428+5G>A]; [2597_2601 delTTTTC]	c.776G>A, homz	c.776G>A, homz	c. 2347_ 2369del, homz	c.2900−1G>A, homz
Variant p. annotation	p.Arg474*, homz	p.[Val257 Glufs*3]; [Val334 Glyfs*19]	p.[Lys447_Arg 476del]; [Leu866 Profs*12]	p.Trp259*, homz	p.Trp259*, homz	p.Leu783Valfs* 5, homz	p.Thr967_ Glu1006 delins Lys, homz
Sex	M	M	F	M	M	F	M
Current age	10 years	8 years	8 years	6 years	10 years	3 years 9 months	19 years
Growth							
Age at measurement	7 years 11 months	8 years	7 years 4 months	6 years	9 years	3 years 9 months	19 years
Height	124 cm (P10–P25)	127 cm (P25)	118.7 cm (P10–P25)	121 cm (P75)	126 cm (P10–P25)	92 cm (P3)	175 cm (P25–P50)
Weight	21 kg (P3–P5)	19.9 kg (P1)	22 kg (P25–P50)	18.3 kg (P25–P50)	17.6 kg (P0.3)	11 kg (P0.5)	63 kg (P25)
OFC	55 cm (P97)	ND	53.5 cm (P50–P75)	ND	ND	47 cm (P10)	ND
Facial features							
Dolichocephaly	+	+	− (prominent sutures)	+	+	−	+
Frontal bossing	+	+	+	+	+	+	−
Hypertelorism	+	+	−	+	+	+	+
Ptosis	+ (L > R)	+ (L > R)	−	−	−	+ (L > R)	+
Retrognathia	+	+	+	−	−	+	+
Submucous cleft palate	−	+ and broad uvula	−	−	−	− and bifid uvula	− and bifid uvula
High arched palate	+	+	+	+	+	−	+
Skeletal findings							
Arachnodactyly	+	+	−	+	+	+	+
Joint hypermobility	+	+	+	+	+	+	+
Pectus excavatum	+	+	+	+	+	+	+
Pes planum	+	+	+	+	+	−	−
Cervical spine anomalies	ND	+	−	ND	−	−	+
Scoliosis	−	+	−	−	+	−	+
Other	2nd toes camptodactyly	kyphosis	recurrent hip and ankle dislocation	talipes equinovarus (L); vertical talus (R)	sagittal clefts of midthoracic vertebrae; talipes equinovarus (R)	−	long toes
Neurological findings							
Hypotonia	+	+	+	+	+	+	+
Developmental delay	+ (mild)	+	+ (motor)	+ (motor)	+ (motor)	+ (motor)	+
Intellectual disability	−	−	−	−	−	mild	+[a]

(*Continued on next page*)

Table 1. *Continued*

	Family 1, proband 1-II:3	Family 2, proband 2-II:1	Family 3, proband 3-II:3	Family 4, proband 4-II:4	Family 4, individual 4-II:3	Family 5, proband 5-II:2	Family 6, proband 6-II:1
Cardiovascular findings							
Age at finding	10 years 8 months	8 years	7 years 5 months	1 year 8 months	9 years	3 years 6 months	19 years
ASD	+	+	+	−	−	+	+ (aneurysmal)
VSD	−	−	+ (membraneous and muscular)	+ (membraneous)	+	+ (membraneous)	−
PDA	−	+	+ (surgical repair)	+	−	−	−
Aortic root	26 mm ($Z = 3.5$)	35 mm ($Z = 10$)	25 mm ($Z = 3.58$)	25 mm ($Z = 5.7$)	38 mm ($Z = 6.0$)	15 mm ($Z = 0,5$)	41 mm ($Z = 6.9$)
Ascending aorta	28 mm ($Z = 5.7$)	28 mm ($Z = 8.7$)	21 mm ($Z = 2.68$)	17 mm ($Z = 3.9$)	23 mm ($Z = 2.7$)	ND	31 mm ($Z = 3.8$)
Sinotubular junction	ND	25 mm ($Z = 5.4$)	23 mm ($Z = 4.99$)	ND	25 mm ($Z = 3.8$)	12 mm ($Z = 0.18$)	23 mm ($Z = 1.2$)
Other aneurysms	ND	com/int carotid, cerebral arteries	ND	ND	ND	pulmonary artery, coronary sinus	ND
Arterial/aortic tortuosity	ND	+	ND	ND	ND	ND	+
Other findings							
Hernia	umbilical	umbilical/bilateral inguinal	−	−	umbilical	umbilical	umbilical/ inguinal
Easy bruising	+	+	−	−	−	−	−

ND, not determined; L, left; R, right; +, present; −, absent; *Z*, *Z* score (calculated according to Lopez et al.);[14] P, percentile; com, common; int, internal; ASD, atrial septal defect; VSD, ventricular septal defect; PDA, patent ductus arteriosus; homz, homozygous; OFC, occipitofrontal circumference.
[a]Proband 6:II-1 also has a chromosomal duplication (1.779 Mb gain of 19q13.41), and learning disability is also present in proband's mother and maternal half-brother.

defects. Evaluation of lateral and dorsoventral total body X-rays, which are publicly available through the International Mouse Phenotyping Consortium (IMPC) portal, did not show evidence for scoliosis (visual inspection) or increased kyphosis (quantitative evaluation; p = 2.8E−1) in *Ipo8*$^{-/-}$ mice as compared to WT animals.

Given the fact that the aneurysmal phenotype is most pronounced in males at the level of the distal ascending aorta, we performed further experiments in male mice only. To study the biomechanical properties of distal ascending aortic rings, we used the "rodent oscillatory tension set-up to study arterial compliance" (ROTSAC) assay.[24] More precisely, *ex vivo* aortic stiffness was assessed at 12 (5 *Ipo8*$^{-/-}$ versus 4 WT), 24 (4 *Ipo8*$^{-/-}$ versus 4 WT), and 52 (4 *Ipo8*$^{-/-}$ versus 2 WT) weeks of age. We used different experimental conditions to evaluate the involvement of vascular smooth muscle cells (VSMCs) and/or endothelial cells. The Peterson modulus (Ep) was first determined in Krebs-Ringer solution at a distention pressure of 80–120 mmHg and 120–160 mmHg, revealing a trend toward higher Ep values and, thus, stiffer ascending aortas at 120–160 mmHg in 12, 24, and 52 week old *Ipo8*$^{-/-}$ male animals as compared to controls (Figures 3 and S8). Because complete VSMC relaxation by diethylamine NONOate (DEANO) addition or VSMC stimulation with phenylephrine (PE), even upon nitric oxide synthase (NOS) inhibition through N(Ω)-nitro-L-arginine methyl ester (L-NAME) addition, did not considerably alter the Ep increase in *Ipo8* null males (Figure 3), neither increased basal tone nor sustained VSMC contraction seem to contribute to the increased aortic stiffness. Our data rather point toward an increased passive stiffness of the ascending aorta in male *Ipo8*$^{-/-}$ mice throughout life. Increased arterial stiffness, an important marker for cardiovascular disease, has previously been observed in genetic TAA mouse models[25] and affected individuals.[26] In an established MFS mouse model, i.e., *Fbn1*$^{mgR/mgR}$, stiffness was augmented in mutant non-aneurysmal (circa 3-fold) and aneurysmal (circa 4-fold) ascending aortas, which upon histological analysis, was shown to correlate with a diffuse loss in elastic fiber integrity.[25] Compared to age-matched controls, TAA-affected individuals exhibit a stiffer mechanical response with aortic biomechanical properties resembling those of a significantly older ("aged") non-aneurysmal cohort.[27] Given the observed trend toward stiffer ascending aortas in *Ipo8*$^{-/-}$ mice (Figure 3) and recurrent prior associations between aortic ECM deterioration and TAA,[2] we evaluated the structural ECM integrity by using histological elastin and collagen staining in ascending aortic sections of 12- (3 *Ipo8*$^{-/-}$ versus 3 WT),

Table 2. Comparison of Marfan, Loeys-Dietz, Sphrintzen-Goldberg, and IPO8 phenotypical characteristics

	MFS	LDS	SGS	IPO8
Gene(s)	*FBN1*	*TGFBR1/2, SMAD2/3, TGFB2/3*	*SKI*	*IPO8*
Inheritance	AD	AD	AD, *de novo*	AR
Ectopia lentis	+++	–	–	–
Cleft palate/bifid uvula	–	++	+	+
Hypertelorism	–	++	++	++
Proptosis	–	+	++	++
Craniosynostosis	–	+	+++	–
Arachnodactyly	+++	++	++	++
Tall stature	+++	+	++	–
Pectus deformity	++	++	++	++
Club foot	–	++	+	+
Joint hypermobility	+	++	++	+++
Cervical spine instability	–	++	+	+
Osteo-arthritis	+	++	+	?
Hernia (umbilical, inguinal …)	+	+	+	+
Aortic root aneurysm	+++	+++	+	+++
Ascending aneurysm	+	++	+	++
Arterial aneurysm	–/+	+++	+	+
Arterial tortuosity	–	+++	+	+
Early aortic dissection	+	++	–	–
BAV/ASD/VSD/PDA	–	+	–	++
Motor developmental delay	–	–	++	++
Intellectual disability	–	–	++	–

–, absent; +, occasional; ++, common; +++, typical clinical feature; ?, unknown; MFS, Marfan syndrome; LDS, Loeys-Dietz syndrome; SGS, Shprintzen-Goldberg syndrome; TAA, thoracic aortic aneurysm; AD, autosomal dominant; AR, autosomal recessive; BAV, bicuspid aortic valve; ASD, atrial septal defect; VSD, ventricular septal defect; PDA, patent ductus arteriosus.

24- (3 *Ipo8*$^{-/-}$ versus 3 WT), and 52-week-old (3 *Ipo8*$^{-/-}$ versus 2 WT) mice. Whereas the collagen content did not differ noticeably (Figure S9A), the elastic fibers were more disorganized and fragmented in mutant males of all age groups as compared to their WT counterparts ($p_{age\text{-}combined} = 5.2E{-}4$) (Figures 4A, 4B, and S9B).

Importin 8 is a nuclear transport receptor belonging to the importin-β protein family, which has not been linked to

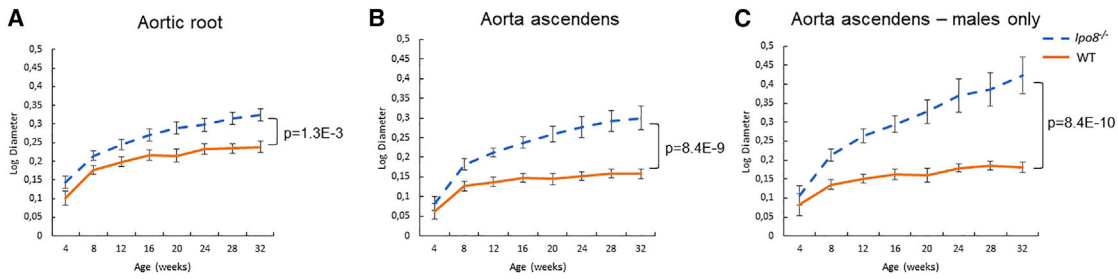

Figure 2. Progressive TAA development in *Ipo8*$^{-/-}$ mice
(A) Log of weight-corrected aortic root diameters in male and female mice combined (N = 17/group).
(B) Log of weight-corrected ascending aortic diameters in male and female mice combined (N = 17/group).
(C) Log of weight-corrected ascending aortic diameters in male mice only (10 *Ipo8*$^{-/-}$ versus 9 WT). The error bars show the standard error of the mean (SEM). p values, which represent the interaction term between genotype and age, were calculated via mixed model analysis. WT, wild-type.

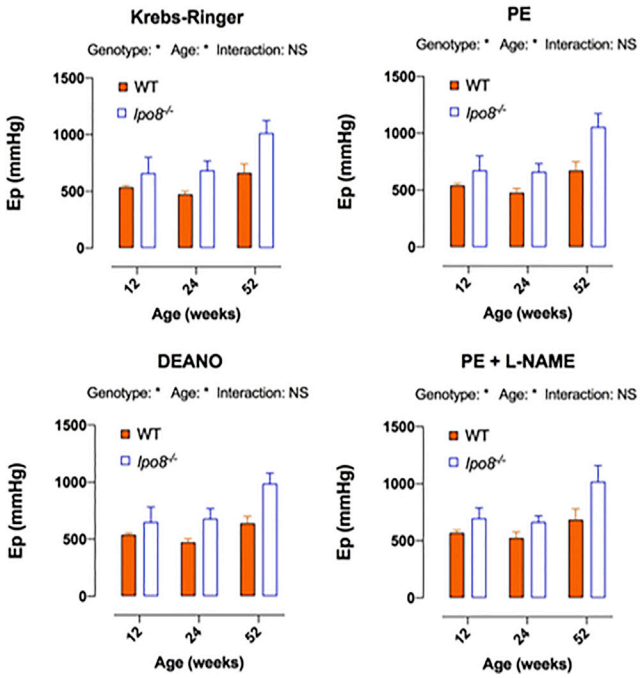

Figure 3. Trend toward increased ascending aortic passive stiffness in *Ipo8*$^{-/-}$ mice at a distention pressure of 120–160 mmHg
Age- and genotype-dependency of the Peterson modulus (Ep) of ascending aortic segments of male *Ipo8*$^{-/-}$ and wild-type mice under control (Krebs-Ringer), maximally relaxed (DEANO), and contracted (PE or PE + L-NAME) conditions at 12 (5 *Ipo8*$^{-/-}$ versus 4 WT), 24 (4 *Ipo8*$^{-/-}$ versus 4 WT), and 52 (4 *Ipo8*$^{-/-}$ versus 2 WT) weeks of age. The error bars show the SEM. Two-way ANOVA p values are shown (*$p < 0.05$). Sidak post hoc testing did not reveal statistically significant genotype-based differences in Ep. PE, phenylephrine; DEANO, diethylamine NONOate; L-NAME, N(Ω)-nitro-L-arginine methyl ester; Ep, Peterson modulus; WT, wild-type; NS, non-significant.

human diseases before. It is ubiquitously expressed and becomes upregulated upon TGF-β1 stimulation.[28] β-importins translocate cargo molecules such as proteins, RNAs, and ribonucleoprotein complexes to the nucleus in a RanGTP-dependent manner. While a specific cargo can be shuttled by multiple β-importins, superior affinity to one of them is often observed. The most established cargoes for human importin 8 are phosphorylated SMADs 1–4 (pSMAD1–4),[29] AGO2,[30] mature miRNAs,[31] EIF4E,[32] and SRP19.[33] Apart from being a nuclear transport receptor, importin 8 has been implicated in miRNA-guided gene silencing.[30] Given that individuals with bi-allelic *IPO8* variants phenotypically resemble individuals with TGF-β-related aortopathy syndromes such as LDS and SGS and key effectors of the canonical TGF-β pathway (i.e., pSMAD2–4) have been reported to be shuttled by importin 8,[29] a plausible hypothesis is that dysregulated TGF-β signaling is involved in the pathogenesis of *IPO8*-related disease (Figure S1). We determined the levels of nuclear pSmad2, an effector of canonical TGF-β signaling, in ascending aortic sections of 12- (3 *Ipo8*$^{-/-}$ versus 3 WT), 24- (3 *Ipo8*$^{-/-}$ versus 3 WT), and 52-week-old (3 *Ipo8*$^{-/-}$ versus 2 WT) mice. A larger fraction of nuclei stained positive for pSmad2 in *Ipo8*$^{-/-}$ mice as compared to WT animals ($p_{age\text{-}combined} = 3.4E{-}2$), suggesting a role for dysregulated TGF-β signaling in the pathogenesis of *IPO8*-related TAA (Figures 4A, 4B, and S9C). Subsequent RT-qPCR analysis for nine TGF-β superfamily-related genes (i.e., *Tgfb1*, *Tgfb2*, *Smad4*, *Smad6*, *Smad7*, *Mmp2*, *Ccn2* [*Ctgf*], *Eln*, and *Serpine1* [*Pai1*]) in ascending aortic samples of 16-week old *Ipo8*$^{-/-}$ and WT males (N = 12/group) revealed significantly reduced *Smad6* ($p = 6.0E{-}3$) and *Smad7* ($p = 3.6E{-}2$) mRNA expression in the mutant animals, along with a significant increase in *Mmp2* ($p = 4.2E{-}3$) and *Ccn2* (*Ctgf*) ($p = 7.8E{-}3$) (Figure 5). SMAD6 and 7 inhibit SMAD-dependent and -independent TGF-β family signaling through various mechanisms.[34] Whereas SMAD6 preferentially inhibits bone morphogenetic protein (BMP)-related signaling,[35] SMAD7 impedes both TGF-β- and BMP-induced signaling.[36] In the absence of SMAD7, TGF-β receptor activation is augmented, resulting in excessive SMAD2/3 phosphorylation. The detected decrease in *Smad7* mRNA levels in the *Ipo8*$^{-/-}$ aortic walls might thus be directly linked to the observed increase in nuclear pSmad2 levels. SMAD6, on the other hand, has mostly been linked to BMP signaling, which is less well studied in the context of TAA development. Nonetheless, our group identified loss-of-function *SMAD6* variants as a cause of bicuspid aortic valve-related TAA,[37,38] demonstrating a mechanistic link between SMAD6 deficiency and TAA development. *MMP2* and *CCN2* (*CTGF*) are prototypical downstream transcriptional targets of the TGF-β signaling pathway.[39] *MMP2* belongs to the family of matrix metalloproteinases, which mediate the physiological turnover of the aortic ECM by degrading structural ECM proteins, including collagen and elastin.[40] In TAA-affected individuals and mouse models, MMP2 levels and/or activity are strongly increased.[41–43] Moreover, *Mmp2* deletion in *Fbn1*$^{mgR/mgR}$ mice inhibited TGF-β activation and subsequent Smad2 and Erk1/2 phosphorylation,[44] which significantly prolonged the lifespan of the MFS *Fbn1*$^{mgR/mgR}$ mice.[44] As such, increased *Mmp2* expression might connect increased TGF-β signaling and impaired elastic fiber integrity in our *Ipo8*$^{-/-}$ mouse model. CCN2 (CTGF) is a multifunctional protein that is involved in ECM remodeling.[39] Overexpression of CCN2 (CTGF) has been proven to be associated with TAA development[45] and has previously been shown to be upregulated in the aortic walls of individuals with LDS.[4,7] Interestingly, elastic fiber fragmentation but normal collagen content as well as reduced *Smad6* and *Smad7* mRNA expression levels and higher Mmp activity were also described in aneurysmal aortic tissue specimens and/or VSMCs of *Smad3*$^{-/-}$ mice, an established LDS model that presents with TAA already at the age of 6 weeks.[46] Together, our histological, immunohistochemistry, and RT-qPCR findings suggest a link between *IPO8* deficiency and dysregulated TGF-β signaling. Moreover, they recapitulate prior observations in an established LDS mouse model, further relating *IPO8*-related TAA to the LDS disease spectrum.

In conclusion, we describe a syndrome caused by bi-allelic loss-of-function variants in *IPO8*. The human and

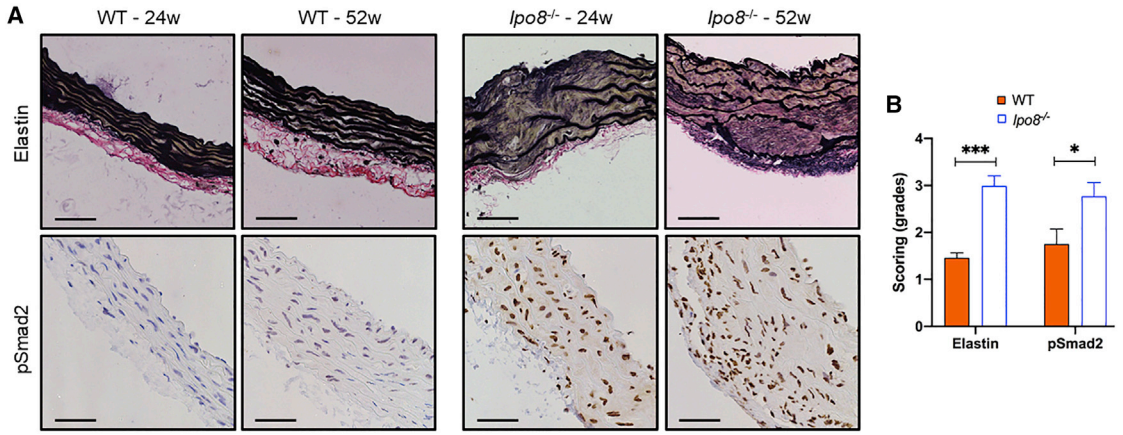

Figure 4. Elastic fiber deterioration and nuclear pSmad2 accumulation in the ascending aorta of *Ipo8*$^{-/-}$ mice
(A) Histological and immunohistochemistry images demonstrating marked elastin disorganization and fragmentation as well as prominent nuclear pSmad2 accumulation in *Ipo8*$^{-/-}$ mice. Scale bar represents 50 μm.
(B) Elastic fiber integrity scores and nuclear pSmad2 grades of the ascending aorta of all ages combined (12 [3 *Ipo8*$^{-/-}$ versus 3 WT], 24 [3 *Ipo8*$^{-/-}$ versus 3 WT], and 52 weeks [3 *Ipo8*$^{-/-}$ versus 2 WT]). Elastin grades can range from 1 to 4: grade 1 sections present with continuous and well-organized elastic bundles and grade 4 sections display vastly disorganized fibers, marked fiber fragmentation, and a thickened aortic wall. For pSmad2, grades 1, 2, 3, and 4 denote sections in which respectively <25%, 25%–50%, 50%–75%, and 75%–100% of nuclei stained positive. Averaged age-combined scores of blinded observations of three independent researchers are shown. The error bars depict the SEM. p values were calculated via two-way ANOVA statistics (*$p < 0.05$, ***$p < 0.001$). WT, wild-type.

mouse phenotypes caused by importin 8 loss of function are characterized by severe early-onset TAA development. Our immunohistochemistry and RT-qPCR studies of murine *Ipo8*-deficient aortic tissue reveal pathophysiological mechanisms that have previously been described in clinically overlapping TGF-β-related signalopathies. Further research is warranted to obtain more in-depth insight into the disease's clinical course and mechanisms. First, identification of additional individuals with bi-allelic *IPO8* variants will shed better light on the variability with respect to disease expressivity and penetrance. Moreover, longitudinal follow-up of affected individuals will provide information on aortic/arterial dissection or rupture risk. Interestingly, our clinical findings are corroborated by the observations of Ziegler et al.,[47] in this issue of *The American Journal of Human Genetics*, who describe aortic dilatation in 11 out of 12 individuals with bi-allelic *IPO8* variants. Second, it remains to be determined whether and how abnormal cytosol-to-nucleus shuttling elicits *IPO8*-related disease and dysregulated TGF-β signaling in aneurysmal aortic walls. Finally, as we predominantly focused on the TAA phenotype, it would be interesting to have a closer look at the mechanisms involved in the other affected organ systems, especially the neuromuscular system in order to explain the motor developmental delay that was observed in individuals with *IPO8* bi-allelic variants.

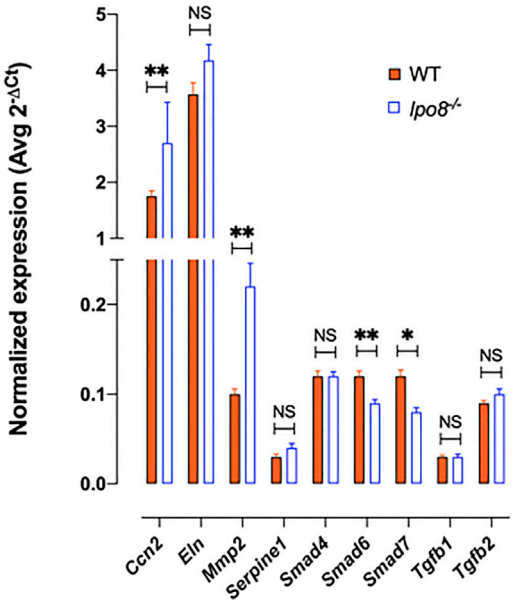

Figure 5. mRNA expression analysis of TGF-β-related genes reveals decreased *Smad6* and *Smad7* levels as well as increased *Mmp2* and *Ccn2 (Ctgf)* levels in the ascending aorta of *Ipo8*$^{-/-}$ mice
Ascending aortic samples of 16-week-old *Ipo8*$^{-/-}$ and WT males were used (N = 12/group). The error bars depict the SEM. p values were calculated via mixed model statistics (*$p < 0.05$, **$p < 0.01$). WT, wild-type; NS, non-significant.

Data and code availability

The *IPO8* variants were submitted to ClinVar (https://www.ncbi.nlm.nih.gov/clinvar/) (GenBank: NM_006390.3; accession numbers SCV001547250–SCV001547257). WES datasets have not been deposited in a public repository because of privacy and ethical restrictions but are available from the corresponding author on request.

Supplemental information

Supplemental information can be found online at https://doi.org/10.1016/j.ajhg.2021.04.019.

Consortia

The members of the Genomics England Research Consortium are John C. Ambrose, Prabhu Arumugam, Marta Bleda, Freya Boardman-Pretty, Christopher R. Boustred, Helen Brittain, Mark J. Caulfield, Georgia C. Chan, Tom Fowler, Adam Giess, Angela Hamblin, Shirley Henderson, Tim J.P. Hubbard, Rob Jackson, Louise J. Jones, Dalia Kasperaviciute, Melis Kayikci, Athanasios Kousathanas, Lea Lahnstein, Sarah E.A. Leigh, Ivonne U.S. Leong, Javier F. Lopez, Fiona Maleady-Crowe, Loukas Moutsianas, Michael Mueller, Nirupa Murugaesu, Anna C. Need, Peter O'Donovan, Chris A. Odhams, Christine Patch, Daniel Perez-Gil, Mariana Buongermino Pereira, John Pullinger, Tahrima Rahim, Augusto Rendon, Tim Rogers, Kevin Savage, Kushmita Sawant, Richard H. Scott, Afshan Siddiq, Alexander Sieghart, Samuel C. Smith, Alona Sosinsky, Alexander Stuckey, Mélanie Tanguy, Ellen R.A. Thomas, Simon R. Thompson, Arianna Tucci, Emma Walsh, Matthew J. Welland, Eleanor Williams, Katarzyna Witkowska, and Suzanne M. Wood.

Acknowledgments

This research was largely supported by funding from the University of Antwerp (Methusalem-OEC grant "Genomed" FFB190208, Hercules grant 30706), the Research Foundation Flanders (FWO, Belgium, G042321N, G040221N, and G044720N), the Dutch Heart Foundation (2013T093), the Belgian Cardiac Surgery Foundation, and the Marfan Foundation. Also, the research was in part supported by the National Institute for Health Research (NIHR) Oxford Biomedical Research Centre based at Oxford University Hospitals NHS Trust and University of Oxford and the Wellcome Trust (203141/Z/16/Z). The views expressed are those of the authors and not necessarily those of the NHS, the NIHR, or the Department of Health. This research was made possible through access to the data and findings generated by the 100,000 Genomes Project. The 100,000 Genomes Project is managed by Genomics England Limited (a wholly owned company of the Department of Health and Social Care). The 100,000 Genomes Project is funded by the National Institute for Health Research and NHS England. The Wellcome Trust, Cancer Research UK, and the Medical Research Council have also funded research infrastructure. The 100,000 Genomes Project uses data provided by persons and collected by the National Health Service as part of their care and support. B.L.L. holds a consolidator grant from the European Research Council (Genomia—ERC-COG-2017-771945). J.A.N.M. (12X8520N) and D.S. (12R5610N) are post-doctoral FWO fellows. I.V.G. (1S70419N), L.V.D.H. (1S81820N), J.D.V. (11C1721N), and C.H.G.N. (1S24 720N) are supported by an FWO PhD fellowship. B.L.L. and A.V. are members of the European Reference Network on rare multisystemic vascular disorders (VASCERN—project ID: 769036, partly cofunded by the European Union Third Health Programme).

Declaration of interests

The Department of Molecular and Human Genetics at Baylor College of Medicine receives revenue from clinical genetic testing conducted at Baylor Genetics Laboratories. A.B. is an employee of GeneDx, Inc.

Received: January 24, 2021
Accepted: April 23, 2021
Published: May 18, 2021

Web resources

GenBank, https://www.ncbi.nlm.nih.gov/genbank/
gnomAD, https://gnomad.broadinstitute.org/
International Mouse Phenotyping Consortium, https://www.mousephenotype.org/
OMIM, omim.org
PDB, www.rcsb.org

References

1. Faggion Vinholo, T., Brownstein, A.J., Ziganshin, B.A., Zafar, M.A., Kuivaniemi, H., Body, S.C., Bale, A.E., and Elefteriades, J.A. (2019). Genes Associated with Thoracic Aortic Aneurysm and Dissection: 2019 Update and Clinical Implications. Aorta (Stamford) *7*, 99–107.
2. Verstraeten, A., Luyckx, I., and Loeys, B. (2017). Aetiology and management of hereditary aortopathy. Nat. Rev. Cardiol. *14*, 197–208.
3. Dietz, H.C., Cutting, G.R., Pyeritz, R.E., Maslen, C.L., Sakai, L.Y., Corson, G.M., Puffenberger, E.G., Hamosh, A., Nanthakumar, E.J., Curristin, S.M., et al. (1991). Marfan syndrome caused by a recurrent de novo missense mutation in the fibrillin gene. Nature *352*, 337–339.
4. Loeys, B.L., Chen, J., Neptune, E.R., Judge, D.P., Podowski, M., Holm, T., Meyers, J., Leitch, C.C., Katsanis, N., Sharifi, N., et al. (2005). A syndrome of altered cardiovascular, craniofacial, neurocognitive and skeletal development caused by mutations in TGFBR1 or TGFBR2. Nat. Genet. *37*, 275–281.
5. Cannaerts, E., Kempers, M., Maugeri, A., Marcelis, C., Gardeitchik, T., Richer, J., Micha, D., Beauchesne, L., Timmermans, J., Vermeersch, P., et al. (2019). Novel pathogenic *SMAD2* variants in five families with arterial aneurysm and dissection: further delineation of the phenotype. J. Med. Genet. *56*, 220–227.
6. Micha, D., Guo, D.C., Hilhorst-Hofstee, Y., van Kooten, F., Atmaja, D., Overwater, E., Cayami, F.K., Regalado, E.S., van Uffelen, R., Venselaar, H., et al. (2015). SMAD2 Mutations Are Associated with Arterial Aneurysms and Dissections. Hum. Mutat. *36*, 1145–1149.
7. van de Laar, I.M., Oldenburg, R.A., Pals, G., Roos-Hesselink, J.W., de Graaf, B.M., Verhagen, J.M., Hoedemaekers, Y.M., Willemsen, R., Severijnen, L.A., Venselaar, H., et al. (2011). Mutations in SMAD3 cause a syndromic form of aortic aneurysms and dissections with early-onset osteoarthritis. Nat. Genet. *43*, 121–126.
8. Boileau, C., Guo, D.C., Hanna, N., Regalado, E.S., Detaint, D., Gong, L., Varret, M., Prakash, S.K., Li, A.H., d'Indy, H., et al.; National Heart, Lung, and Blood Institute (NHLBI) Go Exome Sequencing Project (2012). TGFB2 mutations cause familial thoracic aortic aneurysms and dissections associated with mild systemic features of Marfan syndrome. Nat. Genet. *44*, 916–921.
9. Lindsay, M.E., Schepers, D., Bolar, N.A., Doyle, J.J., Gallo, E., Fert-Bober, J., Kempers, M.J., Fishman, E.K., Chen, Y., Myers, L., et al. (2012). Loss-of-function mutations in TGFB2 cause a syndromic presentation of thoracic aortic aneurysm. Nat. Genet. *44*, 922–927.
10. Bertoli-Avella, A.M., Gillis, E., Morisaki, H., Verhagen, J.M.A., de Graaf, B.M., van de Beek, G., Gallo, E., Kruithof, B.P.T., Venselaar, H., Myers, L.A., et al. (2015). Mutations in a TGF-β ligand, TGFB3, cause syndromic aortic aneurysms and dissections. J. Am. Coll. Cardiol. *65*, 1324–1336.

11. Cannaerts, E., van de Beek, G., Verstraeten, A., Van Laer, L., and Loeys, B. (2015). TGF-β signalopathies as a paradigm for translational medicine. Eur. J. Med. Genet. *58*, 695–703.
12. Doyle, A.J., Doyle, J.J., Bessling, S.L., Maragh, S., Lindsay, M.E., Schepers, D., Gillis, E., Mortier, G., Homfray, T., Sauls, K., et al. (2012). Mutations in the TGF-β repressor SKI cause Shprintzen-Goldberg syndrome with aortic aneurysm. Nat. Genet. *44*, 1249–1254.
13. Schepers, D., Doyle, A.J., Oswald, G., Sparks, E., Myers, L., Willems, P.J., Mansour, S., Simpson, M.A., Frysira, H., Maat-Kievit, A., et al. (2015). The SMAD-binding domain of SKI: a hotspot for de novo mutations causing Shprintzen-Goldberg syndrome. Eur. J. Hum. Genet. *23*, 224–228.
14. Lopez, L., Colan, S., Stylianou, M., Granger, S., Trachtenberg, F., Frommelt, P., Pearson, G., Camarda, J., Cnota, J., Cohen, M., et al.; Pediatric Heart Network Investigators* (2017). Relationship of Echocardiographic *Z* Scores Adjusted for Body Surface Area to Age, Sex, Race, and Ethnicity: The Pediatric Heart Network Normal Echocardiogram Database. Circ Cardiovasc Imaging *10*, e006979.
15. You, K.T., Li, L.S., Kim, N.G., Kang, H.J., Koh, K.H., Chwae, Y.J., Kim, K.M., Kim, Y.K., Park, S.M., Jang, S.K., and Kim, H. (2007). Selective translational repression of truncated proteins from frameshift mutation-derived mRNAs in tumors. PLoS Biol. *5*, e109.
16. Zachariae, U., and Grubmüller, H. (2006). A highly strained nuclear conformation of the exportin Cse1p revealed by molecular dynamics simulations. Structure *14*, 1469–1478.
17. Yamazawa, R., Jiko, C., Choi, S., Park, I.Y., Nakagawa, A., Yamashita, E., and Lee, S.J. (2018). Structural Basis for Selective Binding of Export Cargoes by Exportin-5. Structure *26*, 1393–1398.e2.
18. Koyama, M., Shirai, N., and Matsuura, Y. (2014). Structural insights into how Yrb2p accelerates the assembly of the Xpo1p nuclear export complex. Cell Rep. *9*, 983–995.
19. Dickinson, M.E., Flenniken, A.M., Ji, X., Teboul, L., Wong, M.D., White, J.K., Meehan, T.F., Weninger, W.J., Westerberg, H., Adissu, H., et al. (2016). High-throughput discovery of novel developmental phenotypes. Nature *537*, 508–514.
20. Robinet, P., Milewicz, D.M., Cassis, L.A., Leeper, N.J., Lu, H.S., and Smith, J.D. (2018). Consideration of Sex Differences in Design and Reporting of Experimental Arterial Pathology Studies-Statement From ATVB Council. Arterioscler. Thromb. Vasc. Biol. *38*, 292–303.
21. Anderson, N.K., Juzwiak, E.E., and Dietz, H.C. (2020). A seX(X/Y) Article on Marfan Syndrome. J. Am. Heart Assoc. *9*, e018814.
22. Roman, M.J., Devereux, R.B., Preiss, L.R., Asch, F.M., Eagle, K.A., Holmes, K.W., LeMaire, S.A., Maslen, C.L., Milewicz, D.M., Morris, S.A., et al.; GenTAC Investigators* (2017). Associations of Age and Sex With Marfan Phenotype: The National Heart, Lung, and Blood Institute GenTAC (Genetically Triggered Thoracic Aortic Aneurysms and Cardiovascular Conditions) Registry. Circ Cardiovasc Genet *10*, e001647.
23. Renard, M., Muiño-Mosquera, L., Manalo, E.C., Tufa, S., Carlson, E.J., Keene, D.R., De Backer, J., and Sakai, L.Y. (2017). Sex, pregnancy and aortic disease in Marfan syndrome. PLoS ONE *12*, e0181166.
24. Leloup, A.J., Van Hove, C.E., Kurdi, A., De Moudt, S., Martinet, W., De Meyer, G.R., Schrijvers, D.M., De Keulenaer, G.W., and Fransen, P. (2016). A novel set-up for the ex vivo analysis of mechanical properties of mouse aortic segments stretched at physiological pressure and frequency. J. Physiol. *594*, 6105–6115.
25. Bellini, C., Korneva, A., Zilberberg, L., Ramirez, F., Rifkin, D.B., and Humphrey, J.D. (2016). Differential ascending and descending aortic mechanics parallel aneurysmal propensity in a mouse model of Marfan syndrome. J. Biomech. *49*, 2383–2389.
26. Humphrey, J.D., and Tellides, G. (2019). Central artery stiffness and thoracic aortopathy. Am. J. Physiol. Heart Circ. Physiol. *316*, H169–H182.
27. Sulejmani, F., Pokutta-Paskaleva, A., Ziganshin, B., Leshnower, B., Iannucci, G., Elefteriades, J., and Sun, W. (2017). Biomechanical properties of the thoracic aorta in Marfan patients. Ann. Cardiothorac. Surg. *6*, 610–624.
28. Hu, X., Kan, H., Boye, A., Jiang, Y., Wu, C., and Yang, Y. (2018). Mitogen-activated protein kinase inhibitors reduce the nuclear accumulation of phosphorylated Smads by inhibiting Imp 7 or Imp 8 in HepG2 cells. Oncol. Lett. *15*, 4867–4872.
29. Yao, X., Chen, X., Cottonham, C., and Xu, L. (2008). Preferential utilization of Imp7/8 in nuclear import of Smads. J. Biol. Chem. *283*, 22867–22874.
30. Weinmann, L., Höck, J., Ivacevic, T., Ohrt, T., Mütze, J., Schwille, P., Kremmer, E., Benes, V., Urlaub, H., and Meister, G. (2009). Importin 8 is a gene silencing factor that targets argonaute proteins to distinct mRNAs. Cell *136*, 496–507.
31. Wei, Y., Li, L., Wang, D., Zhang, C.Y., and Zen, K. (2014). Importin 8 regulates the transport of mature microRNAs into the cell nucleus. J. Biol. Chem. *289*, 10270–10275.
32. Volpon, L., Culjkovic-Kraljacic, B., Osborne, M.J., Ramteke, A., Sun, Q., Niesman, A., Chook, Y.M., and Borden, K.L. (2016). Importin 8 mediates m7G cap-sensitive nuclear import of the eukaryotic translation initiation factor eIF4E. Proc. Natl. Acad. Sci. USA *113*, 5263–5268.
33. Dean, K.A., von Ahsen, O., Görlich, D., and Fried, H.M. (2001). Signal recognition particle protein 19 is imported into the nucleus by importin 8 (RanBP8) and transportin. J. Cell Sci. *114*, 3479–3485.
34. Miyazawa, K., and Miyazono, K. (2017). Regulation of TGF-β Family Signaling by Inhibitory Smads. Cold Spring Harb. Perspect. Biol. *9*, a022095.
35. Goto, K., Kamiya, Y., Imamura, T., Miyazono, K., and Miyazawa, K. (2007). Selective inhibitory effects of Smad6 on bone morphogenetic protein type I receptors. J. Biol. Chem. *282*, 20603–20611.
36. Hanyu, A., Ishidou, Y., Ebisawa, T., Shimanuki, T., Imamura, T., and Miyazono, K. (2001). The N domain of Smad7 is essential for specific inhibition of transforming growth factor-beta signaling. J. Cell Biol. *155*, 1017–1027.
37. Gillis, E., Kumar, A.A., Luyckx, I., Preuss, C., Cannaerts, E., van de Beek, G., Wieschendorf, B., Alaerts, M., Bolar, N., Vandeweyer, G., et al.; Mibava Leducq Consortium (2017). Candidate Gene Resequencing in a Large Bicuspid Aortic Valve-Associated Thoracic Aortic Aneurysm Cohort: *SMAD6* as an Important Contributor. Front. Physiol. *8*, 400.
38. Luyckx, I., MacCarrick, G., Kempers, M., Meester, J., Geryl, C., Rombouts, O., Peeters, N., Claes, C., Boeckx, N., Sakalihasan, N., et al. (2019). Confirmation of the role of pathogenic SMAD6 variants in bicuspid aortic valve-related aortopathy. Eur. J. Hum. Genet. *27*, 1044–1053.
39. Lipson, K.E., Wong, C., Teng, Y., and Spong, S. (2012). CTGF is a central mediator of tissue remodeling and fibrosis and its

inhibition can reverse the process of fibrosis. Fibrogenesis Tissue Repair *5* (*Suppl 1*), S24.
40. Van Doren, S.R. (2015). Matrix metalloproteinase interactions with collagen and elastin. Matrix Biol. *44-46*, 224–231.
41. Meffert, P., Tscheuschler, A., Beyersdorf, F., Heilmann, C., Kocher, N., Uffelmann, X., Discher, P., Rylski, B., Siepe, M., and Kari, F.A. (2017). Characterization of serum matrix metalloproteinase 2/9 levels in patients with ascending aortic aneurysms. Interact. Cardiovasc. Thorac. Surg. *24*, 20–26.
42. Wang, C., Chang, Q., Sun, X., Qian, X., Liu, P., Pei, H., Guo, X., and Liu, W. (2015). Angiotensin II Induces an Increase in Matrix Metalloproteinase 2 Expression in Aortic Smooth Muscle Cells of Ascending Thoracic Aortic Aneurysms Through JNK, ERK1/2, and p38 MAPK Activation. J. Cardiovasc. Pharmacol. *66*, 285–293.
43. Chung, A.W., Au Yeung, K., Sandor, G.G., Judge, D.P., Dietz, H.C., and van Breemen, C. (2007). Loss of elastic fiber integrity and reduction of vascular smooth muscle contraction resulting from the upregulated activities of matrix metalloproteinase-2 and -9 in the thoracic aortic aneurysm in Marfan syndrome. Circ. Res. *101*, 512–522.
44. Xiong, W., Meisinger, T., Knispel, R., Worth, J.M., and Baxter, B.T. (2012). MMP-2 regulates Erk1/2 phosphorylation and aortic dilatation in Marfan syndrome. Circ. Res. *110*, e92–e101.
45. Branchetti, E., Poggio, P., Sainger, R., Shang, E., Grau, J.B., Jackson, B.M., Lai, E.K., Parmacek, M.S., Gorman, R.C., Gorman, J.H., et al. (2013). Oxidative stress modulates vascular smooth muscle cell phenotype via CTGF in thoracic aortic aneurysm. Cardiovasc. Res. *100*, 316–324.
46. van der Pluijm, I., van Vliet, N., von der Thusen, J.H., Robertus, J.L., Ridwan, Y., van Heijningen, P.M., van Thiel, B.S., Vermeij, M., Hoeks, S.E., Buijs-Offerman, R.M.G.B., et al. (2016). Defective Connective Tissue Remodeling in Smad3 Mice Leads to Accelerated Aneurysmal Growth Through Disturbed Downstream TGF-β Signaling. EBioMedicine *12*, 280–294.
47. Ziegler, A., Duclaux-Loras, R., Revenu, C., Charbit-Henrion, F., Begue, B., Duroure, K., Grimaud, L., Guihot, A.L., Dumas, V.D., Zarhrate, M., et al. (2021). Bi-allelic variants in IPO8 cause a connective tissue disorder associated with cardiovascular defects, skeletal abnormalities, and immune dysregulation. Am. J. Hum. Genet. Published online May 18, 2021. https://doi.org/10.1016/j.ajhg.2021.04.020.